CLEO CONF 97-18
EPS97 394

Measurement of Inclusive B Decays to the Hyperons Λ, Σ^+, Σ^0, Ξ^-, and Ξ^0

CLEO Collaboration

(July 29, 1997)

Abstract

We report measurements of the branching ratios and momentum distributions of inclusive decays of the B meson into Λ, Σ^+, Σ^0, Ξ^-, and Ξ^0. Using a data sample containing 6.6 million B mesons produced on the $\Upsilon(4S)$ resonance at the CLEO-II experiment at CESR, we obtain branching ratios of (3.42±0.09±0.16)%, (0.97±0.18 ±0.12)% , (0.89±0.15 ±0.11)%, (0.36±0.03 ±0.05)%, and (0.59±0.11±0.11)% respectively. This is the first measurement of the $B \to \Sigma^+ X$, $B \to \Sigma^0 X$, and $B \to \Xi^0 X$ branching ratios.

T. E. Browder,[1] Y. Li,[1] J. L. Rodriguez,[1] T. Bergfeld,[2] B. I. Eisenstein,[2] J. Ernst,[2] G. E. Gladding,[2] G. D. Gollin,[2] R. M. Hans,[2] E. Johnson,[2] I. Karliner,[2] M. A. Marsh,[2] M. Palmer,[2] M. Selen,[2] J. J. Thaler,[2] K. W. Edwards,[3] A. Bellerive,[4] R. Janicek,[4] D. B. MacFarlane,[4] P. M. Patel,[4] A. J. Sadoff,[5] R. Ammar,[6] P. Baringer,[6] A. Bean,[6] D. Besson,[6] D. Coppage,[6] C. Darling,[6] R. Davis,[6] N. Hancock,[6] S. Kotov,[6] I. Kravchenko,[6] N. Kwak,[6] S. Anderson,[7] Y. Kubota,[7] S. J. Lee,[7] J. J. O'Neill,[7] S. Patton,[7] R. Poling,[7] T. Riehle,[7] V. Savinov,[7] A. Smith,[7] M. S. Alam,[8] S. B. Athar,[8] Z. Ling,[8] A. H. Mahmood,[8] H. Severini,[8] S. Timm,[8] F. Wappler,[8] A. Anastassov,[9] J. E. Duboscq,[9] D. Fujino,[9,*] K. K. Gan,[9] T. Hart,[9] K. Honscheid,[9] H. Kagan,[9] R. Kass,[9] J. Lee,[9] M. B. Spencer,[9] M. Sung,[9] A. Undrus,[9,†] R. Wanke,[9] A. Wolf,[9] M. M. Zoeller,[9] B. Nemati,[10] S. J. Richichi,[10] W. R. Ross,[10] P. Skubic,[10] M. Bishai,[11] J. Fast,[11] J. W. Hinson,[11] N. Menon,[11] D. H. Miller,[11] E. I. Shibata,[11] I. P. J. Shipsey,[11] M. Yurko,[11] S. Glenn,[12] S. D. Johnson,[12] Y. Kwon,[12,‡] S. Roberts,[12] E. H. Thorndike,[12] C. P. Jessop,[13] K. Lingel,[13] H. Marsiske,[13] M. L. Perl,[13] D. Ugolini,[13] R. Wang,[13] X. Zhou,[13] T. E. Coan,[14] V. Fadeyev,[14] I. Korolkov,[14] Y. Maravin,[14] I. Narsky,[14] V. Shelkov,[14] J. Staeck,[14] R. Stroynowski,[14] I. Volobouev,[14] J. Ye,[14] M. Artuso,[15] A. Efimov,[15] M. Goldberg,[15] D. He,[15] S. Kopp,[15] G. C. Moneti,[15] R. Mountain,[15] S. Schuh,[15] T. Skwarnicki,[15] S. Stone,[15] G. Viehhauser,[15] X. Xing,[15] J. Bartelt,[16] S. E. Csorna,[16] V. Jain,[16,§] K. W. McLean,[16] S. Marka,[16] R. Godang,[17] K. Kinoshita,[17] I. C. Lai,[17] P. Pomianowski,[17] S. Schrenk,[17] G. Bonvicini,[18] D. Cinabro,[18] R. Greene,[18] L. P. Perera,[18] G. J. Zhou,[18] B. Barish,[19] M. Chadha,[19] S. Chan,[19] G. Eigen,[19] J. S. Miller,[19] C. O'Grady,[19] M. Schmidtler,[19] J. Urheim,[19] A. J. Weinstein,[19] F. Würthwein,[19] D. W. Bliss,[20] G. Masek,[20] H. P. Paar,[20] S. Prell,[20] M. Sivertz,[20] V. Sharma,[20] D. M. Asner,[21] J. Gronberg,[21] T. S. Hill,[21] D. J. Lange,[21] S. Menary,[21] R. J. Morrison,[21] H. N. Nelson,[21] T. K. Nelson,[21] C. Qiao,[21] J. D. Richman,[21] D. Roberts,[21] A. Ryd,[21] M. S. Witherell,[21] R. Balest,[22] B. H. Behrens,[22] W. T. Ford,[22] H. Park,[22] J. Roy,[22] J. G. Smith,[22] J. P. Alexander,[23] C. Bebek,[23] B. E. Berger,[23] K. Berkelman,[23] K. Bloom,[23] D. G. Cassel,[23] H. A. Cho,[23] D. S. Crowcroft,[23] M. Dickson,[23] P. S. Drell,[23] K. M. Ecklund,[23] R. Ehrlich,[23] A. D. Foland,[23] P. Gaidarev,[23] R. S. Galik,[23] L. Gibbons,[23] B. Gittelman,[23] S. W. Gray,[23] D. L. Hartill,[23] B. K. Heltsley,[23] P. I. Hopman,[23] J. Kandaswamy,[23] P. C. Kim,[23] D. L. Kreinick,[23] T. Lee,[23] Y. Liu,[23] G. S. Ludwig,[23] N. B. Mistry,[23] C. R. Ng,[23] E. Nordberg,[23] M. Ogg,[23,**] J. R. Patterson,[23] D. Peterson,[23] D. Riley,[23] A. Soffer,[23] B. Valant-Spaight,[23] C. Ward,[23] M. Athanas,[24] P. Avery,[24] C. D. Jones,[24] M. Lohner,[24] C. Prescott,[24] J. Yelton,[24] J. Zheng,[24] G. Brandenburg,[25] R. A. Briere,[25] A. Ershov,[25] Y. S. Gao,[25] D. Y.-J. Kim,[25] R. Wilson,[25] and H. Yamamoto[25]

---

[*]Permanent address: Lawrence Livermore National Laboratory, Livermore, CA 94551.

[†]Permanent address: BINP, RU-630090 Novosibirsk, Russia.

[‡]Permanent address: Yonsei University, Seoul 120-749, Korea.

[§]Permanent address: Brookhaven National Laboratory, Upton, NY 11973.

[**]Permanent address: University of Texas, Austin TX 78712

[1]University of Hawaii at Manoa, Honolulu, Hawaii 96822
[2]University of Illinois, Champaign-Urbana, Illinois 61801
[3]Carleton University, Ottawa, Ontario, Canada K1S 5B6
and the Institute of Particle Physics, Canada
[4]McGill University, Montréal, Québec, Canada H3A 2T8
and the Institute of Particle Physics, Canada
[5]Ithaca College, Ithaca, New York 14850
[6]University of Kansas, Lawrence, Kansas 66045
[7]University of Minnesota, Minneapolis, Minnesota 55455
[8]State University of New York at Albany, Albany, New York 12222
[9]Ohio State University, Columbus, Ohio 43210
[10]University of Oklahoma, Norman, Oklahoma 73019
[11]Purdue University, West Lafayette, Indiana 47907
[12]University of Rochester, Rochester, New York 14627
[13]Stanford Linear Accelerator Center, Stanford University, Stanford, California 94309
[14]Southern Methodist University, Dallas, Texas 75275
[15]Syracuse University, Syracuse, New York 13244
[16]Vanderbilt University, Nashville, Tennessee 37235
[17]Virginia Polytechnic Institute and State University, Blacksburg, Virginia 24061
[18]Wayne State University, Detroit, Michigan 48202
[19]California Institute of Technology, Pasadena, California 91125
[20]University of California, San Diego, La Jolla, California 92093
[21]University of California, Santa Barbara, California 93106
[22]University of Colorado, Boulder, Colorado 80309-0390
[23]Cornell University, Ithaca, New York 14853
[24]University of Florida, Gainesville, Florida 32611
[25]Harvard University, Cambridge, Massachusetts 02138

I. INTRODUCTION

In B decays, the hyperons Λ, Σ^+,Σ^0, Ξ^-, and Ξ^0 may be produced either from direct B decay or as secondary products of B decays to charmed baryons. Thus the study of inclusive hyperon production in B decays can give important insights into B to charmed baryon decays, as well as into the decay mechanisms of the charmed baryons themselves. The Ξ_c^+ and Ξ_c^0 both have significant decay fractions to both Ξ^- and Ξ^0 as well as smaller ones to Σ^+ and Λ. A significant fraction of the Λ_c^+ baryons decay to Λ, Σ^+, and Σ^0, and a few percent also decay to Ξ^- and Ξ^0.

In Figure 1(a) we show the diagrams of the processes thought to be predominant in B decay to charmed baryons, namely the external spectator diagram, the internal spectator diagram, and the W-exchange diagram. In all three of these mechanisms, the b quark decays to a c quark and a W, and the W fragments to $\overline{u}d$. In these processes if a $u\overline{u}$ or $d\overline{d}$ pair materializes from the vacuum, a charmed baryon Θ_c=(Λ_c^+, Σ_c) will be formed, while a charmed strange Ξ_c baryon will be formed in the case of a $s\overline{s}$ pair. In the latter case a antihyperon $\overline{Y}$ (=$\overline{\Lambda}$, $\overline{\Sigma}$) will also be formed (associated production).

The W can also fragment into $\overline{c}s$, as shown in the diagrams in Figure 1(b). In this case a charmed antibaryon is produced in association with the charmed baryon. If a $b{\to}u$ rather than a $b{\to}c$ transition occurs, a hyperon can be produced in association with the anti-charmed baryon.

It is also possible for hyperon-antihyperon pairs to be produced in association with a D meson. Figure 2(a) shows an external W fragmenting to $\overline{c}s$ with production of a charmed baryon and an antibaryon. This is heavily phase-space suppressed. Figure 2(b) shows a spectator diagram where the external W fragments to a baryon-antibaryon pair. An internal spectator diagram is also possible.

Hyperons can also be signatures for rare charmless decays, as shown in Figure 3. They can be produced in $b \to u$ transitions involving external W, W-exchange, and annihilation diagrams. They can also be products of $b \to s$ penguin diagrams, shown in Figure 3(b).

CLEO has previously observed inclusive B decays to the charmed baryons Λ_c^+ [1], Σ_c [2], and Ξ_c [3], which together account for several percent of the total B decay rate. The $B \to \Lambda X$ rate was measured to be $(3.8 \pm 0.4 \pm 0.6)\%$ [1]. CLEO has also previously measured [1] the branching ratio of $B \to \Xi^- X$ to be $(0.27 \pm 0.06)\%$ and ARGUS reports [4] a branching ratio of $B \to \Xi^- X$ of $(0.28 \pm 0.14)\%$. We present here the first measurement of the $B \to \Xi^0 X$, $B \to \Sigma^+ X$ and $B \to \Sigma^0 X$ branching fractions.

The diagrams shown in Figure 1(a) are expected to dominate hyperon production in B decays, although Dunietz argues that the D baryon-antibaryon rate may be enhanced due to charmed baryon excitations above the $D\overline{p}$ threshold [5]. Most theoretical predictions [6–16] predict only two-body exclusive states, which are unobservable given the current level of data. In an early paper, Bigi [17] estimated the inclusive rate of charmed baryon production in B decays to be between 2 and 13%.

The diagrams in Figure 1 indicate that in $\overline{B}$ decays (B^- or $\overline{B}^0$), the $b{\to}cW$ transition leads to the production of Λ_c^+ and Ξ_c preferentially over $\overline{\Lambda}_c^-$ and $\overline{\Xi}_c$. Thus we should expect hyperons predominantly from $\overline{B}$ decays. A recent CLEO study of this correlation [18] showed that for $\overline{B}{\to}\Lambda_c^+ X$ decays this was the case, but that there was evidence for $\overline{\Lambda}$ and $\overline{\Lambda}_c^-$ production from $\overline{B}$ decays as well. Since we do not fully reconstruct the B mesons in this analysis, we are unable to determine their charge and flavor content. Therefore the notation $B \to Y\ \mathrm{X}$ used in this paper should be understood to include contributions from $\overline{B}$ and B decays, and to include both hyperons and antihyperons.

II. CLEO II EXPERIMENT

A. Detector

The CLEO II detector is described in detail elsewhere [19]. We will describe briefly the parts of the detector relevant to this analysis. The CLEO II detector is designed to detect both charged and neutral particles with excellent resolution and efficiency. The detector consists of a charged particle tracking system surrounded by a scintillation-counter-based time-of-flight system and an electromagnetic calorimeter consisting of 7800 thallium-doped cesium iodide crystals. The tracking system, time-of-flight scintillators and calorimeter are installed inside a 1.5 T superconducting solenoidal magnet. The momentum resolution of the tracking system is given by $(\delta p/p)^2 = (0.15p\%)^2 + (0.5\%)^2$, where p is the track momentum in GeV/c. Charge measurements from the drift chamber wires provide specific ionization loss (dE/dx) information. The photon energy resolution achieved by the electromagnetic calorimeter [20] varies from 4.2% at 100 MeV to 1.4% at 5 GeV.

B. Particle Identification

To identify hadrons, dE/dx and time-of-flight (TOF) measurements (if available) are combined to define a joint $\chi^2_i = [\{(dE/dx)_{\mathrm{meas}} - (dE/dx)_{\mathrm{exp}}\}/\sigma_{dE/dx}]^2_i + [\{(T)_{\mathrm{meas}} - (T)_{\mathrm{exp}}\}/\sigma_{\mathrm{TOF}}]^2_i$, where i corresponds to the pion, kaon, and proton hypotheses. A χ^2-probability is then calculated for each hypothesis. By itself, the dE/dx measurement provides two standard deviation π/K separation up to 0.7 GeV/c. Time-of-flight measurements extend the two standard deviation π/K separation up to 1.1 GeV/c and two standard deviation p/K separation up to 1.7 GeV/c. A charged track is defined to be consistent with a pion (proton) hypothesis, if its probability to be a pion (proton) is greater than 0.001.

C. Data Sample

We use 4.7 fb^{-1} of integrated luminosity. Of this, 3.1 fb^{-1} is on the $\Upsilon(4S)$ resonance and 1.6 fb^{-1} is just below the threshold for $B\overline{B}$ production. This sample contains 6.6 million B mesons. We refer to these data samples as on-resonance and off-resonance in further discussions.

For the inclusive Λ analysis, a smaller data sample was used consisting of an integrated luminosity of 2.27 fb^{-1} taken at the $\Upsilon(4S)$ resonance, and 1.08 fb^{-1} taken in the region of energy below the $\Upsilon(4S)$ resonance. This sample contains 4.8 million B mesons.

III. ANALYSIS PROCEDURE

The goal of this analysis is to measure the inclusive production of hyperons from B decay, that is, $B \to \Lambda X$, $B \to \Sigma^+ X$, $B \to \Sigma^0 X$, $B \to \Xi^- X$, and $B \to \Xi^0 X$, where X stands for a combination of an antibaryon and mesons. The data on the $\Upsilon(4S)$ contains hyperons from both B decays and continuum production. B decays are characterized by a more spherical event shape as measured by the Fox-Wolfram second moment r_2 [21], and by lower momentum of the decay products. Since events in the continuum are more jetty, its contribution can be suppressed by requiring $r_2 < 0.35$. We use the normalized momentum $x_p = p/p_{max}$ where $p_{max} = \sqrt{E_B^2 - m_\Upsilon^2}$. Since a hyperon from B decay is kinematically limited to about $x_p < 0.4$, we only consider inclusive hyperon production in this region.

In order to isolate the contribution of hyperons produced in B decays from those produced in continuum processes, we subtract the invariant mass distribution found in the off-resonance data from that of the on-resonance data, with appropriate scaling. This procedure is done in each x_p interval.

Below, we first present the reconstruction techniques for each of the hyperons, that is $\Lambda \to p\pi^-$, $\Sigma^+ \to p\pi^0$, $\Sigma^0 \to \Lambda\gamma$, $\Xi^- \to \Lambda\pi^-$, and $\Xi^0 \to \Lambda\pi^0$. We then discuss the procedure for obtaining the raw and corrected yields for each hyperon as a function of x_p. Discussion of the Monte Carlo simulation to estimate the reconstruction efficiency is also included. The results of the measurements are then presented.

A. Hyperon Reconstruction

1. Reconstruction of Λ

We form Λ candidates from pairs of oppositely charged tracks, assumed to be a p and a π^-. The p track is required to be consistent within four standard deviations of the proton hypothesis. If dE/dx information is available for the pion, we require the probability that it is a pion to be greater than 0.001. In order to reduce the background, we require the distance of the Λ vertex from the beam line to be greater than 2 mm. The Λ candidates are required to have an invariant mass within ± 5 MeV/c^2 of the known Λ mass. A Λ decays to $p\,\pi^-$ $(63.9\pm0.5)\%$ of the time [22].

For the inclusive Λ analysis, the impact parameters in the xy plane for both the proton and the pion are required to be over three standard deviations from the origin, instead of requiring the vertex distance to be greater than 2 mm. Only specific ionization measurements from the central drift chamber were used for particle identification, and $K_s^0 \to \pi^-\pi^+$ background is explicitly removed by excluding the $\pi^+\pi^-$ mass region (0.485–0.510 GeV/c^2) when the proton candidate is interpreted as a pion. Figure 4(a) shows the invariant mass distributions of all $p\pi^-$ combinations with $x_p < 0.4$ for both the on and off-resonance samples.

2. Reconstruction of Σ^+

The candidates for Σ^+ are reconstructed by combining a p and a π^0. The π^0 candidates are formed from a pair of photon candidates. One of the photon candidates is required to originate from the barrel CsI crystals, i.e., to have $|cos(\theta)| < 0.707$, where θ is the angle of the photon with respect to the beam direction. The photons are required to deposit at least 30 MeV of energy in the CsI crystals. Any showers that are matched to charged tracks projected into the calorimeter are excluded. We perform a kinematic fit of the two photons, constraining them to have the π^0 mass, and require $\chi^2_{\pi^0} < 10$ for the kinematic fit. We select showers consistent with photons based on the ratio of the energy of the nine crystals closest to the shower center to that of the twenty-five closest crystals (E9/E25 cut).

To isolate Σ^+ candidates, stronger particle identification is required. The particle identification level=$P(\chi^2_p)/(P(\chi^2_p) + P(\chi^2_K) + P(\chi^2_\pi))$ for the proton is required to be greater than 0.1. To reduce the combinatorial background, we further require that the momentum of the proton be greater than 400 MeV/c and that of the pion greater than 100 MeV/c.

The Σ^+ is formed by combining the momentum of the p with the π^0 momentum as calculated under the assumption the π^0 comes from the primary vertex. Then we find the Σ^+ decay vertex by finding the intersection point of the Σ^+ track and the proton track. We then refit the π^0 to originate at this vertex point and calculate the invariant mass of the $p\pi^0$ combination. Figure 5(a) shows the invariant mass of $p\pi^0$ combinations for x_p< 0.4, for both the on and off-resonance samples.

3. Reconstruction of Σ^0

The Σ^0 candidates are reconstructed by combining a Λ and a γ. We require the photon energy to be greater than 500 MeV/c^{2}to reduce background from unrelated soft photons. We apply an E9/E25 cut on the photon, as described above. The $\Lambda\gamma$ invariant mass distributions for $x_p < 0.4$ are shown in Figure 5(b), for both the on and off-resonance samples.

4. Reconstruction of Ξ^-

The Ξ^- candidates are formed by pairing a Λ candidate with a negatively charged track in the event, assumed to be a π^-. If dE/dx information is available for the π^- track, it is required to have a probability of at least 0.001 of being a pion. These tracks are required to fit a 3-dimensional vertex in space. The radial distance of the Ξ^- from the beamline is required to be less than the Λ distance, and greater than 2 mm. The Ξ^- track is required to point back to the event vertex and the π^- track is required to not point back to the event vertex. The measured z positions of the Λ and π^- tracks must be within 2 cm of each other. Figure 6(a) shows the invariant mass distributions of all $\Lambda\pi^-$ combinations with $x_p < 0.4$.

5. *Reconstruction of* Ξ^0

The Ξ^0 is formed by combining a Λ and a π^0. The π^0 candidates are selected as described in the Σ^+ reconstruction above. The Ξ^0 is formed by combining the momentum of the Λ with the π^0 momentum as calculated under the assumption that the π^0 comes from the primary vertex. Then we find the Ξ^0 decay vertex by finding the intersection point of the Ξ^0 and the Λ. It is possible to correct the π^0 and Λ momenta to come from this vertex and re-iterate the calculation but it has been found to be unnecessary. The reconstructed Ξ^0 is required to have a radial distance from the beamline of at least 5 mm. Figure 6(b) shows the invariant mass distributions of all $\Lambda\pi^0$ combinations with $x_p < 0.4$.

B. Monte Carlo Simulation

We perform a Monte Carlo simulation of our detector's response to $B \to \Sigma^+ X$ and $B \to \Sigma^0 X$ events. The simulation begins with B^- and $\overline{B}^0$ decays to charmed baryons where $B\to\Lambda_c^+\overline{p}\mathrm{n}(\pi)$ (15%), $B\to\Lambda_c^+\overline{\Lambda}K^-\mathrm{n}(\pi)$(2%), $B\to\Lambda_c^+\overline{\Sigma}K^-\mathrm{n}(\pi)$(4%), $B\to\Sigma_c\overline{p}\mathrm{n}(\pi)$(12%), $B\to\Xi_c\overline{\Lambda}\mathrm{n}(\pi)$(33%), $B\to\Xi_c\overline{\Sigma}\,\mathrm{n}(\pi)$(13%), and $B\to\Xi_c\overline{\Lambda}_c^-\mathrm{n}(\pi)$(17%). The other B meson decays generically. n can be from 0 to 6 charged pions and can also include a π^0. We also include 4% of two-body direct decays such as $B\to\Xi_c\overline{\Sigma}$. The charmed baryons are forced to decay into channels which include a Σ^+ or Σ^0 and the light quarks are allowed to hadronize generically. This mix of final states produces multiplicity and momentum distributions similar to those observed in the data.

For the simulation of $B \to \Xi^- X$ and $B \to \Xi^0 X$ we begin with $\overline{B}\to \Xi_c X$ using final states of the form $B\to\Xi_c\overline{\Lambda}\mathrm{n}(\pi)$ (70%) and $B\to\Xi_c\overline{\Lambda}_c^-\mathrm{n}(\pi)$ (30%) where n can stand for 0 through 4 charged pions and a π^0. The Ξ_c then decays into Ξ^- and Ξ^0 with the light quarks hadronizing generically.

In the simulation of the $B \to \Lambda X$ decay, a generic B Monte Carlo was used which included a phenomenological model based on a previous CLEO measurement [1].

We use the Monte Carlo to find the expected shape and width of the mass distributions, both for all data with $x_p < 0.4$ and in Δx_p intervals of 0.1 from $0 < x_p < 0.1$, $0.1 < x_p < 0.2, \cdots$ to $0.3 < x_p < 0.4$, for all particles except Λ, where intervals of 0.03 are used. The information from the Monte Carlo is used to determine the shapes of both the on-resonance and the off-resonance mass distributions.

The detection efficiencies are obtained by dividing the fitted signal areas from the Monte Carlo simulation by the number of events generated in each x_p interval. The efficiencies for each x_p interval, corrected for the branching fractions $\mathrm{B}(\Sigma^+ \to p\pi^0) = (51.57\pm0.30)\%$, $\mathrm{B}(\Sigma^0 \to \Lambda\gamma) \approx 100\ \%$ and $\mathrm{B}(\Lambda \to p\pi^-) = (63.9\pm 0.5)\%$ [22], are shown in Tables I,II,III, IV, and V for Λ, Σ^+,Σ^0, Ξ^-, and Ξ^0 respectively.

C. Continuum Subtraction

We scale the off-resonance data to account for the quadratic energy dependence of the continuum cross section and the difference in integrated luminosity between it and the on-resonance data. To obtain the yields of hyperons from B decays, we subtract the scaled off-resonance sample from the on-resonance sample, and fit the resulting mass distribution in intervals of x_p. Subtracting the results of separate fits to the two samples yields a consistent result, providing a useful check of the technique.

D. Fitting Procedure

The raw yield of events in each x_p interval is obtained by fitting the subtracted invariant mass distributions to the sum of a Gaussian function and a low-order polynomial background. The mean mass is constrained to the value derived from a fit to the invariant mass distribution integrated from $0.0 < x_p < 0.4$. The width of the Gaussian signal function is further constrained to the value predicted by the Monte Carlo simulation for hyperons reconstructed in the appropriate momentum interval.

We divide the raw yield by the efficiency to obtain the corrected yield. We sum the corrected yields from each momentum bin up to $x_p \leq 0.4$, and divide by the total number of B mesons, $N_B = (6.60 \pm 0.09) \times 10^6$, to obtain the branching ratio. We plot the differential yield as a function of x_p by dividing each yield by the x_p interval, 0.1 for all cases except Λ where it is 0.03.

E. Systematic Errors

We estimate the systematic errors by tightening the r_2 cuts to 0.25 and observing the variation of the answers. In all cases the answers are consistent. The comparison of fitting the continuum-subtracted histogram to subtracting the fitted yields shows that these two methods give consistent answers. We find the systematic error in reconstruction efficiencies for Λ, Ξ^-, and Ξ^0 to be (4%, 3%, and 7%) respectively. For Σ^0 there are additional errors in determining the background shape (5%) and in photon reconstruction efficiency (5%). The major Σ^+ systematics include the uncertainty in particle identification efficiency (5%) and π^0 reconstruction efficiency (5%).

In the $B \to \Lambda X$ analysis, estimates of the main sources of systematic error include tracking (3%), fits to the $p\pi$ mass distributions (2%, except for $0.03 < x_p < 0.06$, where the fit error is conservatively estimated at 30%), number of produced B's (1.8%), modeling of the vertex-finding efficiency (1.5%), Monte Carlo statistics (2%), particle identification (1%), and the error involved in extrapolating the x_p distribution to zero (0.3%). In addition, for each bin, there is a systematic error due to feed-in from Λ with mismeasured momenta, which is conservatively taken to be 100% of the actual correction, making it typically 2% for each bin, but approximately 35% for the bin $0.03 < x_p < 0.06$. Thus for each bin the systematic error is obtained separately by adding the contributions in quadrature. The total systematic error in $\langle n_\Lambda \rangle$ is about 5%.

F. Results

The results of our measurements of inclusive production of Λ, Σ^+, Σ^0, Ξ^-, and Ξ^0 in B decays are presented in Tables I,II,III, IV, and V respectively. The corresponding momentum distributions are plotted in Figure 4(b) for Λ, Figure 5(c) and (d) for Σ^+ and Σ^0, and Figure 6(c) and (d) for Ξ^- and Ξ^0. In each table we tabulate for each x_p interval the raw number of events from the fit, the efficiency, the corrected yield, and the differential yield normalized to N_B and the bin width.

A feature of the data that is as yet unexplained is the fact that the $B \to \Xi^0 X$ branching ratio is 1.6 times that of the $B \to \Xi^- X$ branching ratio. The most likely method of Ξ^- and Ξ^0 production is decay from the Ξ_c^0 and Ξ_c^+ charmed baryons, which were recently observed in B decay by CLEO [3]. This effect could be explained if one of the Ξ_c charge states could be shown to be more dominant in B decay, and it decayed preferentially to Ξ^0 over Ξ^-. Unfortunately, the relative abundance of $\overline{B} \to \Xi_c^0 X$ and $\overline{B} \to \Xi_c^+ X$ remains unknown due to the large errors of the measured branching ratios [3] and the unknown correction factors which are different for the two particles. Several large branching fractions have been observed in $\Xi_c^+ \to \Xi^0(\mathrm{n}\pi)$ as opposed to only one in $\Xi_c^+ \to \Xi^- \pi^+ \pi^+$ [23], but it is not yet clear whether this is only because the Ξ^0 channels are easier to find or are actually enhanced relative to the Ξ^- channels.

In general, the momentum distributions of the hyperons seen here are quite soft, showing that multi-body decay dominates not only in the decay of the B meson but also in the decay of the charmed baryons.

IV. CONCLUSION

We have measured the following branching ratios:

$$B \to \Lambda X = (3.42 \pm 0.09 \pm 0.16)\%$$

$$B \to \Sigma^+ X = (0.97 \pm 0.18 \pm 0.12)\%$$

$$B \to \Sigma^0 X = (0.89 \pm 0.15 \pm 0.11)\%$$

$$B \to \Xi^- X = (0.36 \pm 0.03 \pm 0.05)\%$$

$$B \to \Xi^0 X = (0.59 \pm 0.11 \pm 0.11)\%$$

where the first error is statistical and the second is systematic. The $B \to \Lambda X$ and $B \to \Xi^- X$ branching fractions are consistent with the previous measurements. These are the first measurements of $B \to \Sigma^+ X$, $B \to \Sigma^0 X$, and $B \to \Xi^0 X$. Since Σ^0, Ξ^0, and Ξ^- all decay to Λ nearly 100% of the time, we can calculate the amount of direct Λ not coming from heavier hyperons to be $(1.58 \pm 0.30 \pm 0.22)\%$. Also we note that the $B \to \Sigma^+ X$ and $B \to \Sigma^0 X$ branching ratios are similar. If the unmeasured $B \to \Sigma^- X$ branching ratio is also similar then the total $B \to \Sigma X$ branching ratio would be about 80% of the inclusive $B \to \Lambda X$ ratio.

We gratefully acknowledge the effort of the CESR staff in providing us with excellent luminosity and running conditions. This work was supported by the National Science Foundation, the U.S. Department of Energy, the Heisenberg Foundation, the Alexander von Humboldt Stiftung, the Natural Sciences and Engineering Research Council of Canada, and the A.P. Sloan Foundation.

REFERENCES

[1] G. Crawford *et al.* Phys. Rev. D 45, 752 (1992).
[2] M. Procario *et al.* Phys. Rev. Lett **73**, 1472-1476 (1994).
[3] B. Barish *et al.*, CLNS 97/1470 (1997).
[4] Albrecht *et al.*, Z. Phys. C. **42**, 519 (1989).
[5] I. Dunietz FERMILAB-PUB-96/104-T (1996).
[6] I. Dunietz *et al.* Phys. Rev. Lett 73:1075-1078, (1994).
[7] J. G. Korner, Z. Phys. C43, 165 (1989).
[8] M. Jarfi, O. Lazrak, A. Le Yaouanc, L. Oliver, O. Pene, J.C. Rayna, Phys. Rev. D43, 1599-1632 (1991).
[9] T. Mannel, W. Roberts, Z. Ryzak, Phys. Rev. D45, 875-878 (1992).
[10] S. M. Sheikholeslami, M. P. Khanna, Phys. Rev. D44, 770-774 (1991).
[11] G. Kaur, M. P. Khanna, Phys. Rev. D46, 466-469 (1992).
[12] V. L. Chernyak and I. R. Zhitnitsky, Munich High Energy Physics 1988:494, (1988).
[13] M. J. Savage and M. B. Wise, Nucl. Phys. B326, 15 (1989).
[14] V. L. Chernyak and I. R. Zhitnitsky, Nucl. Phys. B345, 137 (1990).
[15] Y. Kohara, Il Nuovo Cimento, 104A, 555 (1991).
[16] P. Ball and H. G. Dosch, Z. Phys. C51, 445 (1991).
[17] I. I. Bigi, Phys. Lett. 106B, 510 (1981).
[18] R. Ammar *et al.* (CLEO), Phys. Rev. D **55**, 13 (1997).
[19] Y. Kubota et al, Nucl. Inst. and Meth. A 320, 66 (1992).
[20] E. Blucher et al, Nucl. Inst. and Meth. A 249, 201 (1989).
[21] G. C. Fox and S. Wolfram, Phys. Rev. Lett., **41**, 1581 (1978).
[22] Particle Data Group, R.M. Barnett *et al.*, Phys. Rev. D **54**, 1 (1996).
[23] K. Edwards et al, Phys. Lett. B 373, 362 (1996).

TABLE I. Inputs to the calculation of $\langle n_\Lambda \rangle$ and $(1/N_B)$ $d(B \to \Lambda X)/dx$ distribution data points. The efficiencies include the $\Lambda \to p\pi$ branching ratio.

x_p Range	Raw Yield	Efficiency(%)	Corrected Yield	$\frac{1}{N_B} \frac{dn}{dx}(B \to \Lambda X)$
$0.03 < x_p < 0.06$	75 ± 28	0.012	6233 ± 2369	$0.0427 \pm 0.0162 \pm 0.0202$
$0.06 < x_p < 0.09$	1621 ± 99	0.051	31537 ± 1930	$0.2161 \pm 0.0132 \pm 0.0107$
$0.09 < x_p < 0.12$	4014 ± 152	0.089	44900 ± 1703	$0.3077 \pm 0.0117 \pm 0.0151$
$0.12 < x_p < 0.15$	3842 ± 170	0.121	31716 ± 1405	$0.2173 \pm 0.0096 \pm 0.0107$
$0.15 < x_p < 0.18$	3271 ± 172	0.146	22345 ± 1178	$0.1531 \pm 0.0081 \pm 0.0075$
$0.18 < x_p < 0.21$	2306 ± 165	0.166	13887 ± 995	$0.0952 \pm 0.0068 \pm 0.0047$
$0.21 < x_p < 0.24$	1446 ± 159	0.181	7974 ± 879	$0.0546 \pm 0.0060 \pm 0.0027$
$0.24 < x_p < 0.27$	536 ± 157	0.193	2768 ± 812	$0.0190 \pm 0.0056 \pm 0.0012$
$0.27 < x_p < 0.30$	660 ± 149	0.203	3249 ± 735	$0.0223 \pm 0.0050 \pm 0.0014$
$0.30 < x_p < 0.33$	236 ± 138	0.212	1117 ± 649	$0.0077 \pm 0.0044 \pm 0.0004$
$0.33 < x_p < 0.36$	79 ± 125	0.220	360 ± 569	$0.0025 \pm 0.0039 \pm 0.0001$
$0.36 < x_p < 0.39$	-42 ± 113	0.227	-186 ± 496	$-.0013 \pm 0.0034 \pm 0.0001$
$0.39 < x_p < 0.42$	18 ± 96	0.235	75 ± 150	$0.0005 \pm 0.0010 \pm 0.0000$
$0.42 < x_p < 0.45$	85 ± 90	0.244	349 ± 368	$0.0024 \pm 0.0025 \pm 0.0001$
$0.45 < x_p < 0.48$	-61 ± 77	0.254	-238 ± 305	$-.0016 \pm 0.0021 \pm 0.0001$
$0.48 < x_p < 0.51$	-103 ± 70	0.266	-389 ± 262	$-.0027 \pm 0.0018 \pm 0.0001$
	$17983\pm$ 682		165697 ± 4458	$\langle n_\Lambda \rangle = (3.42 \pm 0.09 \pm 0.16)\%$

TABLE II. $B \to \Sigma^+ X$ **Summary Table**

x_p Range	Raw Yield	Efficiency(%)	Corrected Yield	$\frac{1}{N_B}\frac{dY}{dx}$ (x 10^{-2})
$0.0 < x < 0.1$	425±150	1.62 ±0.27	26140±10177	3.961±1.542
$0.1 < x < 0.2$	2406±384	7.98±0.49	30149±5152	4.568±0.781
$0.2 < x < 0.3$	1091±337	10.20±0.83	10689±3416	1.620±0.518
$0.3 < x < 0.4$	-358±290	13.65±1.40	-2620±2144	-0.397±0.325
$0 < x < .4$	3716 ±591		64359 ±12099	$\langle n_{\Sigma^+} \rangle = (0.97 \pm 0.18 \pm 0.12)\%$

TABLE III. $B \rightarrow \Sigma^0 X$ **Summary Table**

x_p Range	Raw Yield	Efficiency(%)	Corrected Yield			$\frac{1}{N_B}\frac{dY}{dx}$ (x 10^{-2})
$0.0 < x < 0.1$	1700±291	5.07 ±0.89	33551 ±8219			5.084 ±1.245
$0.1 < x < 0.2$	22354 ±4532	10.15 ±0.64	22354 ±4532			3.387 ±0.687
$0.2 < x < 0.3$	6112 ±2849	15.69 ±1.63	6112 ±2849			0.926 ±0.432
$0.3 < x < 0.4$	-600 ±-3163	18.99 ±2.67	-3163 ±1965			-0.479 ±0.298
$0.0 < x < 0.4$	4327±773		58855±10003	$\langle n_{\Sigma^0} \rangle$	=	$(0.89 \pm 0.15 \pm 0.11)\%$

TABLE IV. $B \rightarrow \Xi^- X$ **Summary Table**

x_p Range	Raw Yield	Efficiency(%)	Corrected Yield			$\frac{1}{N_B}\frac{dY}{dx}$ (x 10^{-2})
$0.0 < x < 0.1$	137 ±25	1.63 ±0.12	8405 ±1654			1.273 ±0.251
$0.1 < x < 0.2$	789 ±63	6.15 ±0.22	12829 ±1122			1.944 ±0.170
$0.2 < x < 0.3$	270 ±66	9.82 ±0.60	2749 ±693			0.417 ±0.105
$0.3 < x < 0.4$	–65±50	15.5 ±2.4	–419 ±355			–0.063±0.054
$0.4 < x < 0.5$	11 ±40	8.75 ±0.45	128 ±458			0.019 ±0.069
$0.5 < x < 0.6$	–7±25	8.52 ±0.51	–82 ±293			0.012 ±0.044
$0.0 < x < 0.4$	1131±107		23564 ±2145	$\langle n_{\Xi^-} \rangle$	=	$(0.36 \pm 0.03 \pm 0.05)\%$

TABLE V. $B \rightarrow \Xi^0 X$ **Summary Table**

x_p Range	Raw Yield	Efficiency(%)	Corrected Yield			$\frac{1}{N_B}\frac{dY}{dx}$ (x 10^{-2})
$0.0 < x < .1$	161 ±50	0.98 ±0.19	16429 ±6015			2.489 ±0.911
$0.1 < x < 0.2$	793 ±105	4.24 ±0.32	18703 ±2850			2.834 ±0.432
$0.2 < x < 0.3$	186 ±95	6.49 ±0.82	2866 ±1508			0.434 ±0.228
$0.3 < x < 0.4$	80 ±74	5.56 ±2.59	1439 ±1490			0.218 ±0.226
$0.4 < x < 0.5$	24 ±53	4.51 ±0.36	532 ±1176			0.081 ±0.178
$0.5 < x < 0.6$	–18±30	3.61 ±0.36	–499 ±833			–0.076±0.126
$0.0 < x < 0.4$	1220±167		39437 ±6985	$\langle n_{\Xi^0} \rangle$	=	$(0.59 \pm 0.11 \pm 0.11)\%$

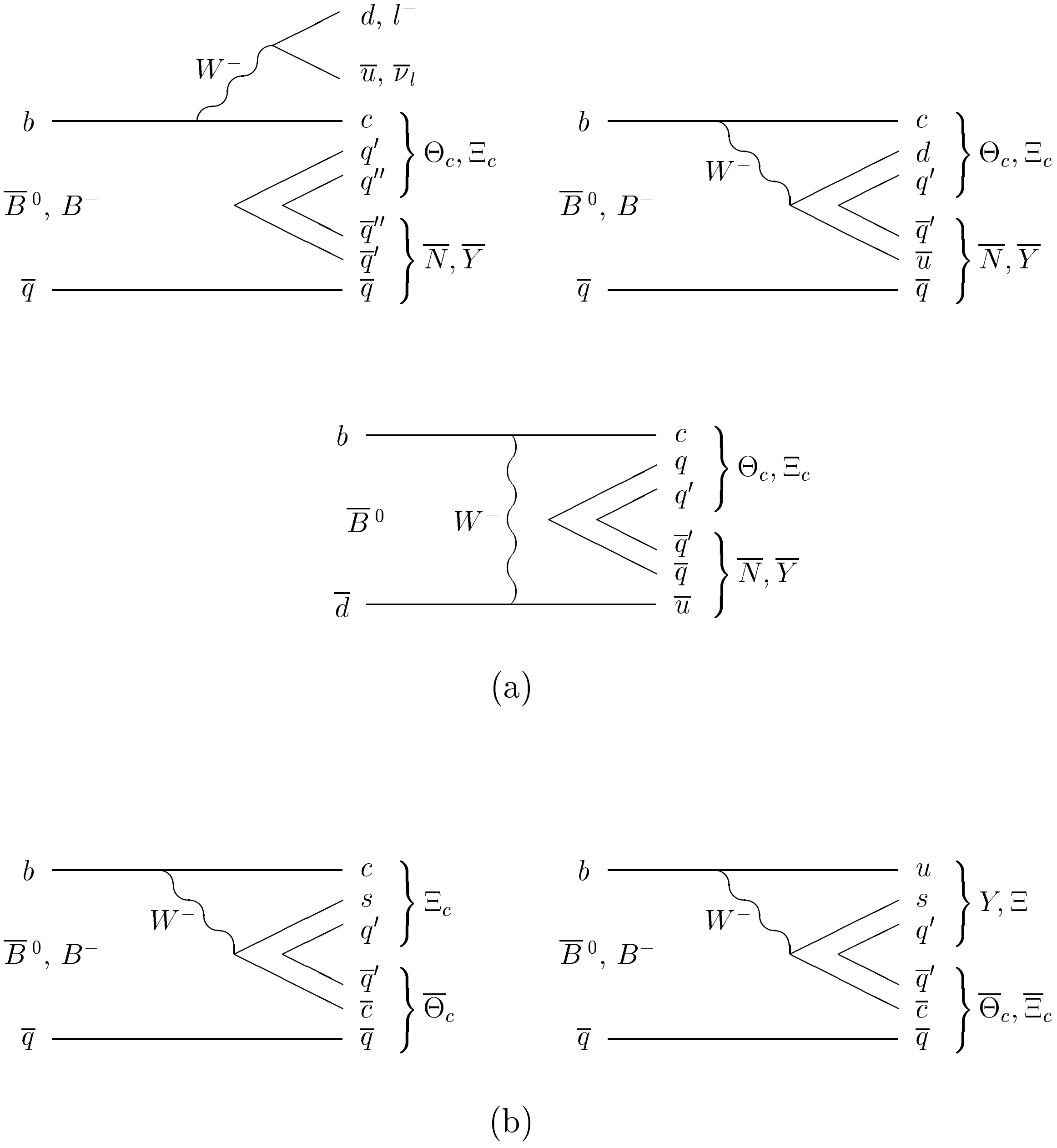

FIG. 1. Possible $B \to$ baryon decay mechanisms: (a) $\overline{B} \to \Theta_c \overline{N} X$ and $\Xi_c \overline{Y} X$, (b) $\overline{B} \to \Xi_c \overline{\Theta}_c X$ and $\overline{B} \to Y \overline{\Theta}_c X$ and $\Xi \overline{\Xi}_c X$.

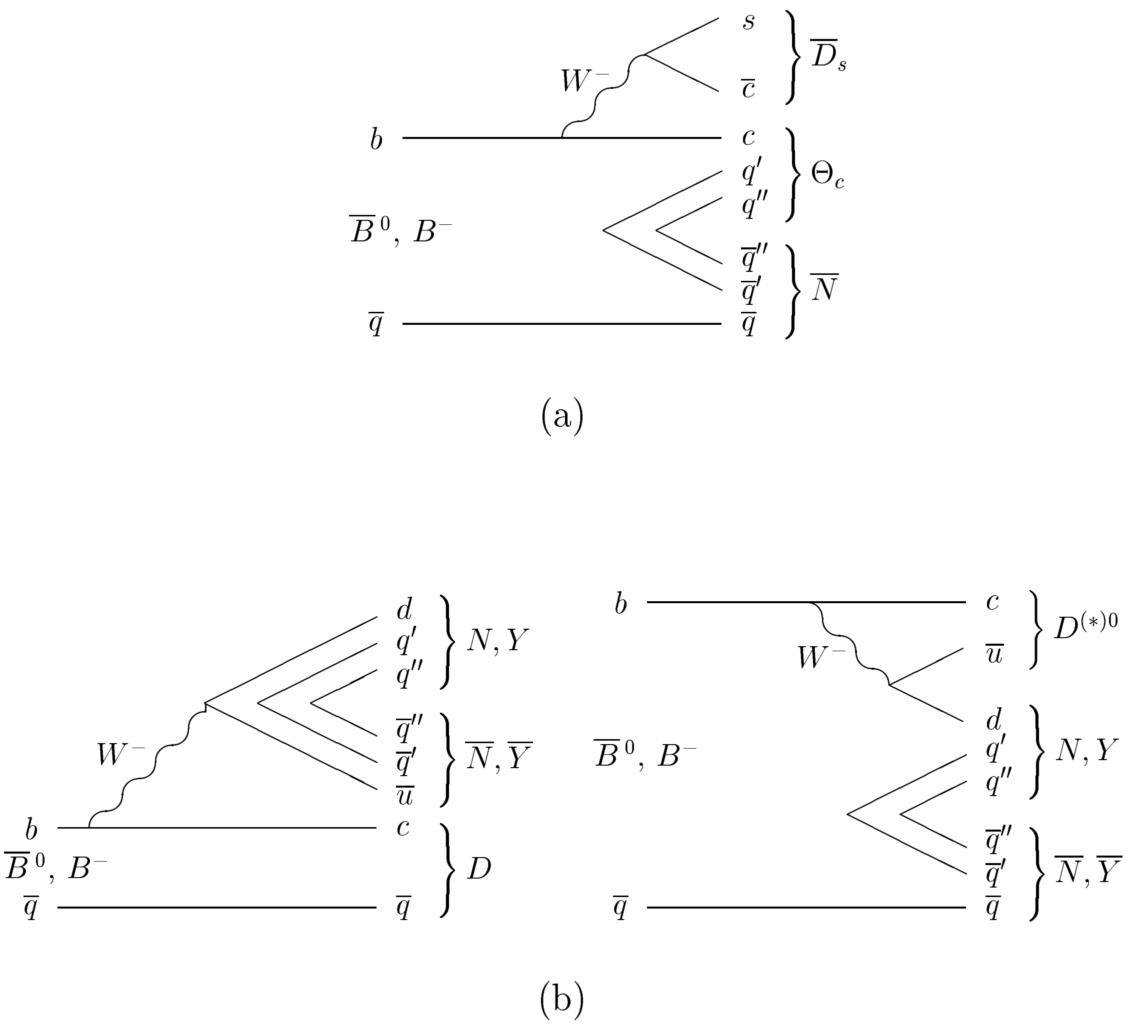

FIG. 2. Possible $B \to$ baryon decay mechanisms (continued): (a) $\overline{B} \to \overline{D}_s \Theta_c \overline{N} X$ and $\overline{D}_s \Xi_c \overline{Y} X$, (b) $\overline{B} \to D N \overline{N} X$ and $D Y \overline{Y} X$.

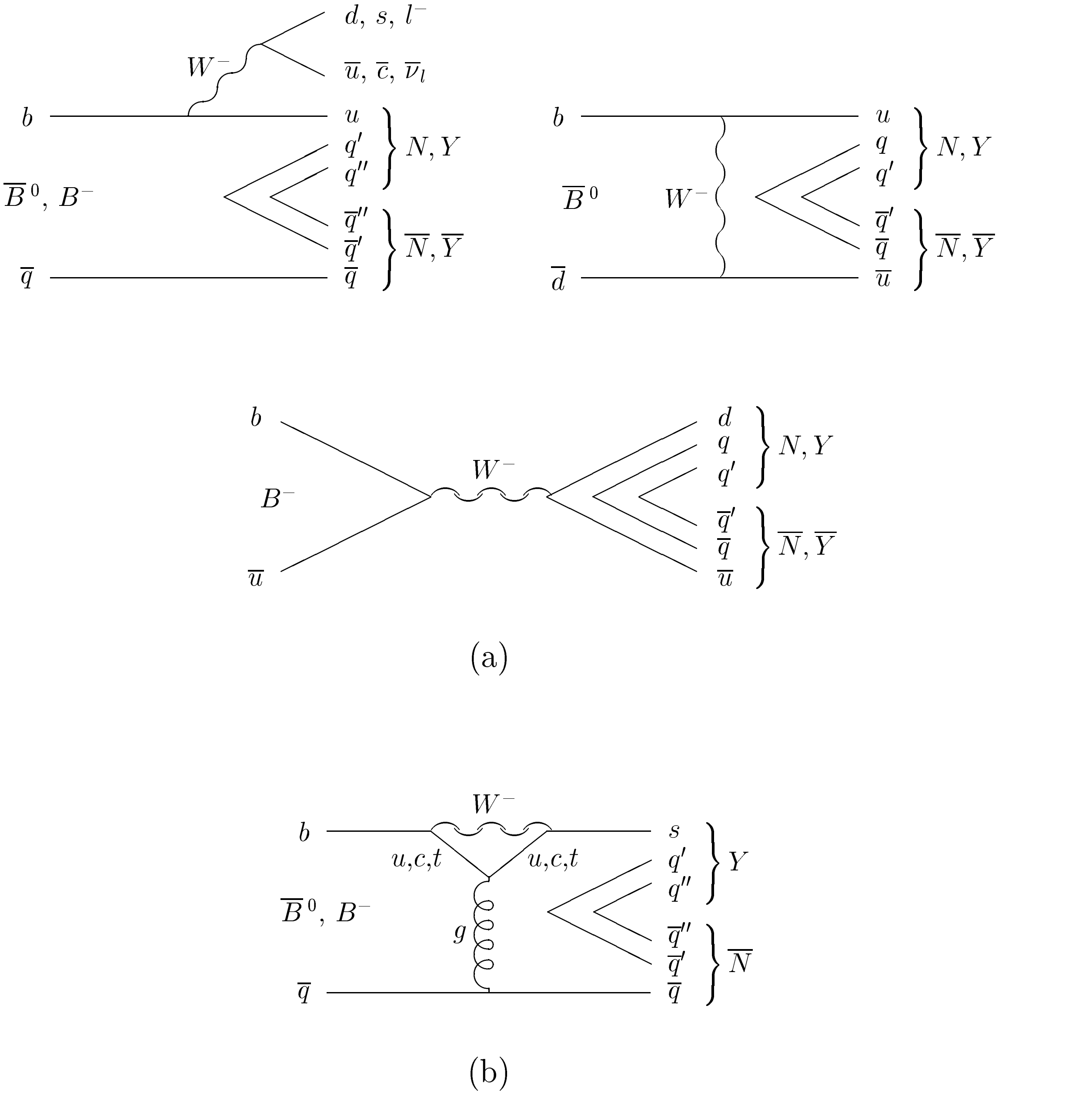

FIG. 3. Possible $B \to$ baryon decay mechanisms (continued): (a) $\overline{B} \to N\overline{N}X$ and $Y\overline{Y}X$, (b) $\overline{B} \to Y\overline{N}X$.

(a)

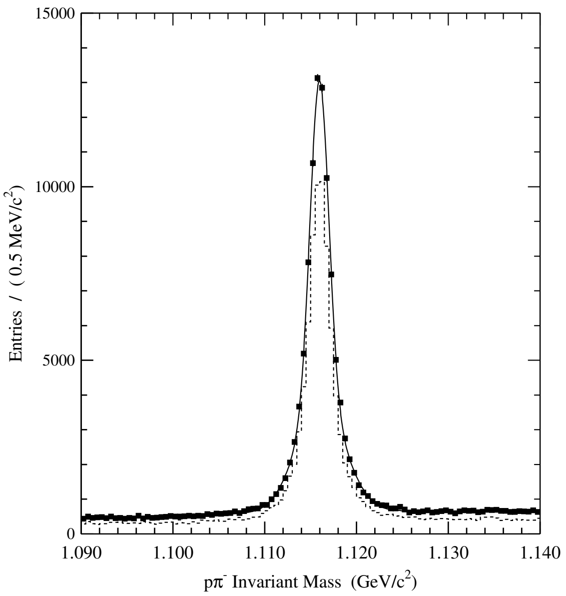

(b)

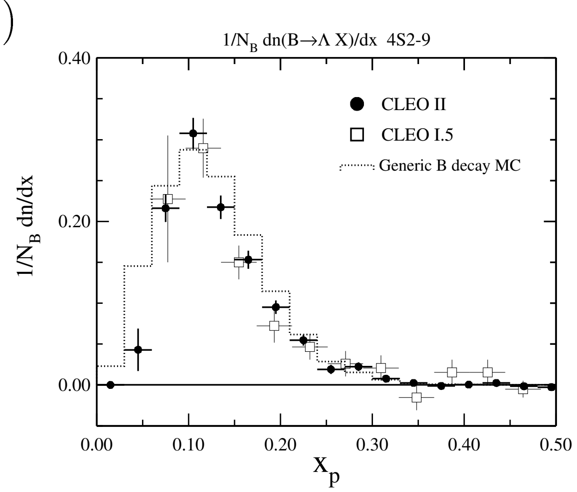

FIG. 4. (a)Invariant mass distribution for $p\pi^-$ combinations, for $r_2 < 0.35$ and x_p<0.4, corresponding to data from the $\Upsilon(4S)$ (data points) and from the scaled continuum (dotted histogram). (b) The $(1/N_B)d(B \to \Lambda X)/dx$ distribution for this experiment, *CLEO I*.5 [1], and generic B decay MC.

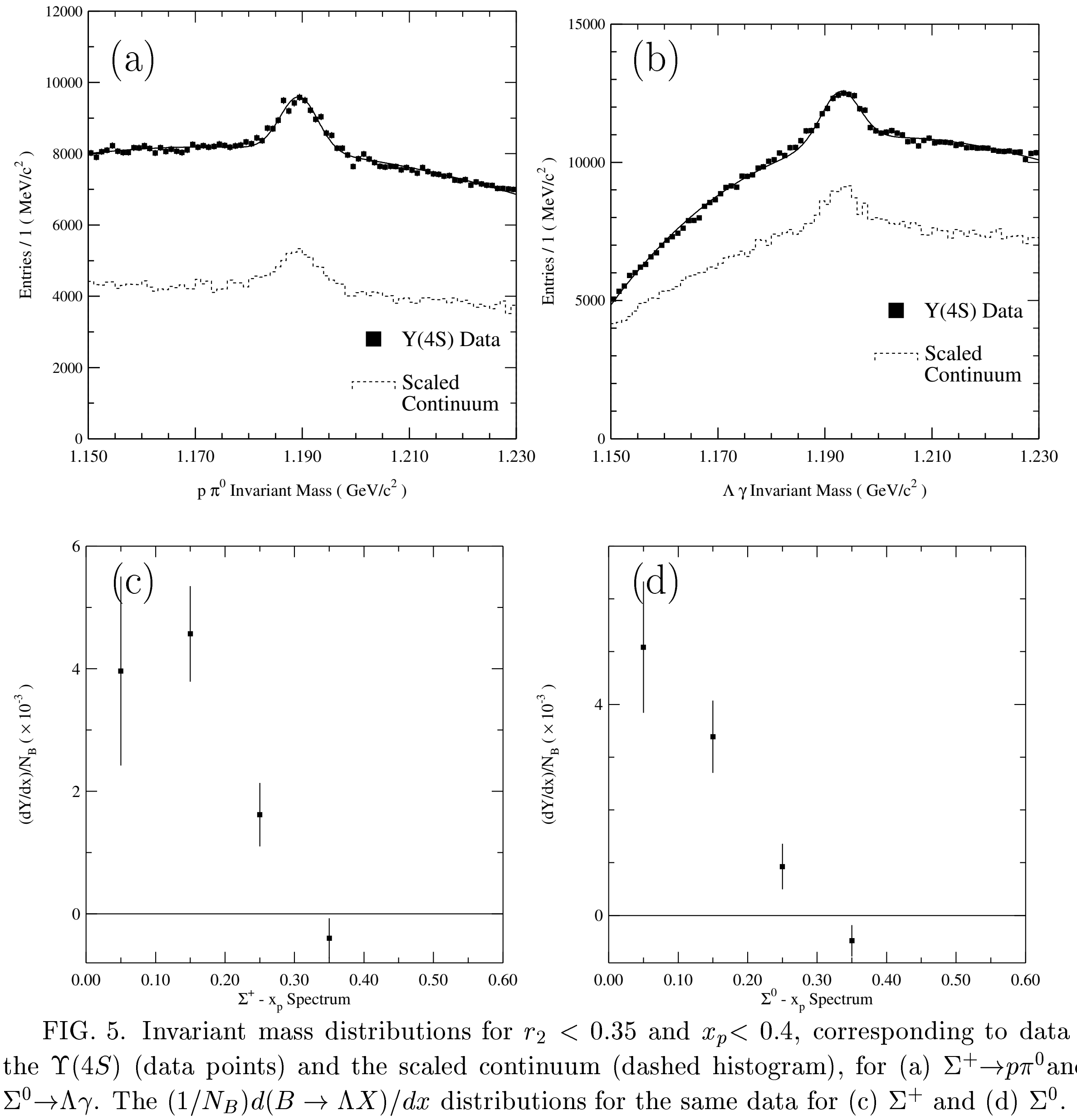

FIG. 5. Invariant mass distributions for $r_2 < 0.35$ and $x_p < 0.4$, corresponding to data from the $\Upsilon(4S)$ (data points) and the scaled continuum (dashed histogram), for (a) $\Sigma^+ \to p\pi^0$and (b) $\Sigma^0 \to \Lambda\gamma$. The $(1/N_B)d(B \to \Lambda X)/dx$ distributions for the same data for (c) Σ^+ and (d) Σ^0.

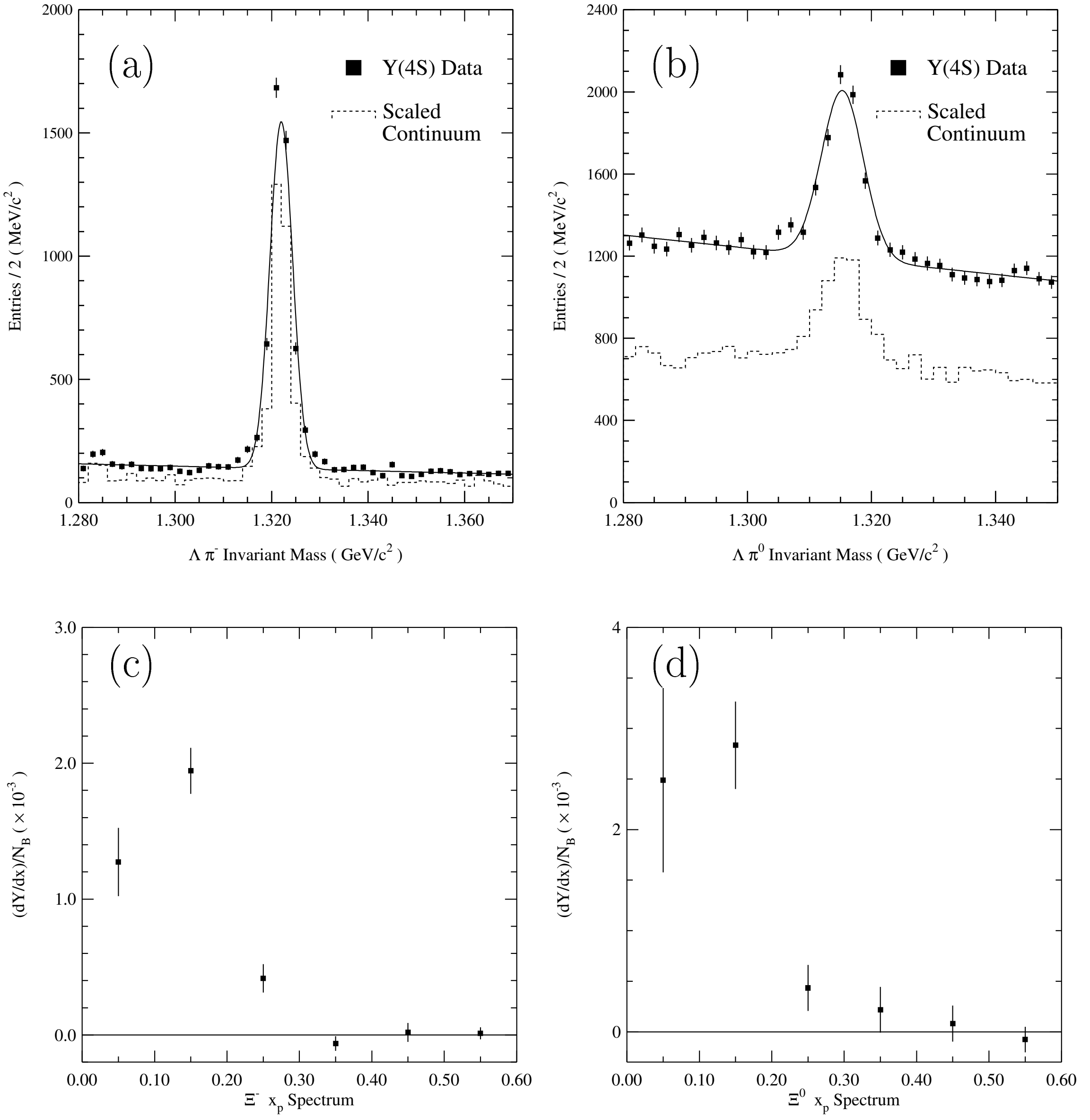

FIG. 6. Invariant mass distributions for $r_2 < 0.35$ and $x_p < 0.4$, corresponding to data from the $\Upsilon(4S)$ (data points) and the scaled continuum (dashed histogram), for (a) $\Xi^- \to \Lambda\pi^-$ and (b) $\Xi^0 \to \Lambda\pi^0$. The $(1/N_B)d(B \to \Lambda X)/dx$ distributions for the same data for (c) Ξ^- and (d) Ξ^0.